ACS SENSORS

pubs.acs.org/acssensors Article

Wearable Plant Sensor for In Situ Monitoring of Volatile Organic Compound Emissions from Crops

Hussam Ibrahim,[§] Satyanarayana Moru,[§] Patrick Schnable, and Liang Dong*

Cite This: https://doi.org/10.1021/acssensors.2c00834 Read Online

ACCESS | Metrics & More | Article Recommendations | Supporting Information

ABSTRACT: Methanol is a major volatile organic compound (VOC) emitted from plants. Methanol emission reflects indirect plant defense against insects, promotes cell-to-cell communication, and adapts plants to various environmental stresses. This paper reports a wearable plant sensor that can monitor methanol emission directly on the leaf of a plant under field conditions with low cost, high portability, and easy installation and use. The sensor technology eliminates the need for complex sampling, expensive instruments, and skilled operators for conventional gas chromatography-mass spectrometry. The sensor uses a composite of conducting polymer microcrystallites and platinum nanoparticles (PtNPs). The conducting poly(2-amino-1,3,4-thiadiazole) or poly(ATD) provides a high electrocatalytic activity with redox behavior. The modification of poly(ATD) with catalytic PtNPs enables efficient electrochemical oxidation of methanol at a specific potential. The advantages of poly(ATD) and PtNPs are synergized for high sensitivity and selectivity of the sensor for detecting methanol emissions with a sub-ppm limit of detection. Further, the infusion of a polymer electrolyte into the porous electrode of the sensor enables an all-solid-state VOC sensor. The sensor is integrated into a miniature gas collection chamber and capped with a hydrophobic gas diffusion membrane to minimize the influence of environmental humidity on the sensor performance. The sensor is installed on the leaf surface. In situ detection shows a difference in methanol emission between the lower and upper leaves of greenhouse maize plants. Further, under field conditions, the sensor reveals a noticeable difference in methanol emission concentration between two genotypes (Mo17 and B73 inbred lines) of maize plants. Therefore, the sensor will provide a promising new means of directly monitoring volatile emission of plants, which is a physiological phenotype as a function of genes and environment.

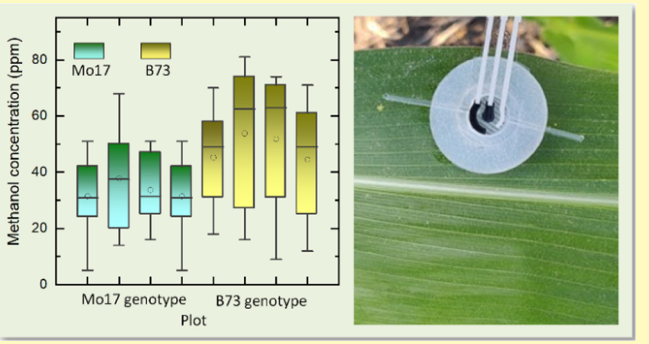

KEYWORDS: *wearable plant sensor, organic volatiles, methanol, agricultural sensor*

Wearable sensors have been extensively studied for biomedical and healthcare applications. Integration of flexible and stretchable electronics with nanomaterials has led to a suite of wearable sensors to monitor vital symptoms, assess responses, and provide treatment.[1,2] Recently, plant wearable sensors have attracted increasing attention because they can monitor many physiological parameters that are critical for a better understanding of how genotypes interact with their environments, thus contributing to plant breeding to address future challenges in ensuring food security in a changing climate.[3] For example, an on-leaf plant sensor was reported to continuously monitor transpiration and water use in maize plants.[4] An ultrasonic transducer[5] and a chemoresistive sensor array[6] were developed to detect volatiles from plants. Also, carbon nanotube-based infrared fluorescent nanosensors with specific peptides enabled the monitoring of contaminant nitroaromatics in leaf tissues.[7] In conjunction with remote sensing methods, these sensors are promising to realize multimodal monitoring of plant growth, stresses, and diseases at a large scale.

Plants emit many volatile organic compounds (VOCs) as indicators of plant defense against insects, pollinator attraction, plant-to-plant communication, environmental stress adaptation, and defense from predators.[8] Also, VOC emission can be induced by nutrient deficiencies, mineral toxicities, lack or excess of soil moisture and nutrients, and improper use of agrochemicals.[9] Therefore, analyzing VOC emissions from plants will be beneficial to the understanding of the physiological status of the plants under various biotic and abiotic stresses. Presently, gas chromatography-mass spectrometry (GC-MS)[10] and proton-transfer-reaction mass spectrometry[11] are common techniques for plant VOC analysis with

Received: April 17, 2022
Accepted: July 27, 2022

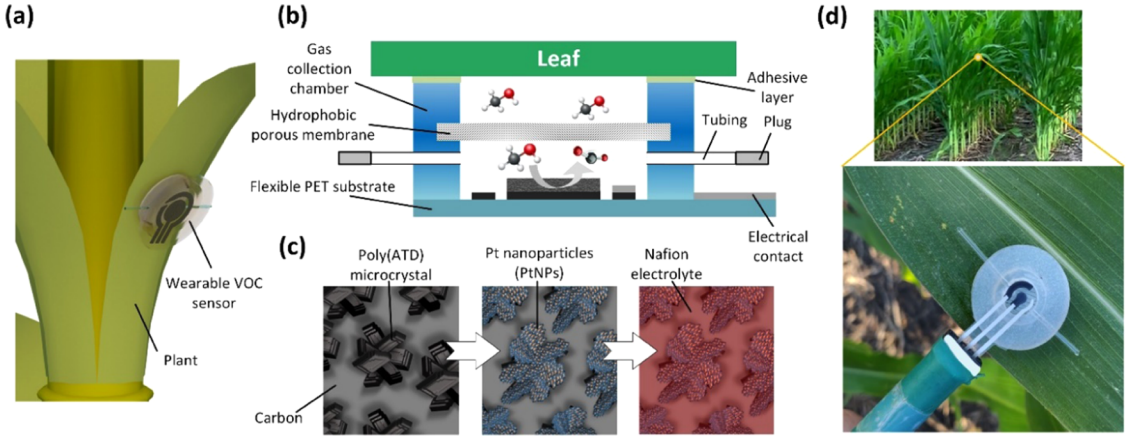

Figure 1. (a) Schematic of the VOC sensor installed on the surface of a leaf. (b) Cross-sectional view of the methanol sensor. (c) Conducting poly(ATD) electrodeposited on the surface of a carbon electrode (left), modified with platinum nanoparticles (middle), and infused with the Nafion-based solid-state polymer electrolyte (right). (d) Photograph of the VOC sensor installed on the leaf surface.

high selectivity; this method, however, requires complex gas sampling processes, intensive labor, expensive instruments, and skilled operators, thus making it not suitable for in-field measurement. Profoundly, low-cost, miniature VOC sensors have a great potential to be a portable solution to on-site VOC analysis under field conditions. These sensors work on the principles of the optical nose,[12] metal oxide semiconductors,[13] electronic nose,[14] photoionization,[15] microelectromechanical systems,[16] electrochemical[17] and chemoresistive transducers,[18] and colorimetry.[19] Among various VOC sensor technologies, electrochemical detection of volatile compounds with conducting polymers and nanomaterials has been extensively investigated and demonstrated as a promising method for biomedical, environmental, and industrial applications. Despite the progress on miniature VOC sensors, it is still in the infancy stage of developing and deploying wearable sensors for monitoring VOC emissions from plants.[19−23]

Methanol has an average concentration second only to methane among atmospheric hydrocarbons.[24] More than 60% of the total source of global methanol arises from the terrestrial biosphere and primary emissions from plants, generally exceeding emissions of all other VOCs except terpenoids.[24] As a regular product of metabolism, methanol is emitted from plants through the biochemical process of methylation and demethylation of RNA, DNA, and protein.[25] For example, methanol serves as a priming stimulus when released from wounded tobacco leaves by enhancing antibacterial defenses in neighboring non-wounded plants against the pathogenic bacterium *Ralstonia solanacearum*;[26] this volatile compound can also promote cell-to-cell communication to facilitate the spread of tobacco mosaic virus in neighboring plants.[26] In addition, methanol production from plants is affected by temperature, light, water status, stomatal conductance, and growth stage.[27] Therefore, monitoring methanol emissions from plants can help to provide valuable information on plant growth, health, and stress.[28] Such an ability, however, has rarely been realized.

This paper reports a wearable electrochemical VOC sensor for on-leaf monitoring of methanol emission from maize (Figure 1a,b). The sensor is structured primarily with three carbon electrodes patterned on a flexible substrate, where the central carbon electrode is modified with a composite of conducting polymer and platinum nanoparticles (PtNPs). The conducting polymer used here is poly(2-amino-1,3,4-thiadiazole) or poly(ATD) formed via electrochemical potentiodynamic polymerization of monomer ATD. Poly(ATD) is chosen over many other conducting polymers (e.g., polypyrrole, polyaniline, polythiophene, etc.) because its monomer state, i.e., 1,3,4-thiadiazole monomers, is electron deficient due to the electron-withdrawing effect of the nitrogen atom. The electron deficiency of the monomers facilitates electron transfer by absorbing more electrons upon a chemical reaction. Also, 1,3,4-thiadiazole monomers are steady in acidic media,[29] which makes this monomer suitable to form a conducting polymer via electrochemical polymerization. In addition, 1,3,4-thiadiazole monomers can act as well-known ligands for bridging metal centers with Co(II). These traits make 1,3,4-thiadiazole monomers promising in electrocatalysis for developing new composites with metal nanoparticles such as PtNPs. Here, poly(ATD) has microcrystallite-like structures that can improve the kinetics of electrode processes because these microcrystallites have high electrocatalytic activity with redox behavior.[29] To improve electrochemical oxidation of methanol, poly(ATD) is further modified with PtNPs as a catalyst (Figure 1c), where the microcrystallites-like structures of poly(ATD) provide a high surface area for hosting more PtNPs and serve as conductive linkages between PtNPs and a carbon electrode.[30−32] A synergy between the poly(ATD) and PtNPs enables sensitive and selective detection of methanol emissions from plants. To realize an all-solid-state sensor, Nafion, a polymer electrolyte, is infused into the pores of the central carbon electrode (Figure 1c). Further, the sensor is integrated into a gas collection chamber capped with a hydrophobic gas diffusion membrane (Figure 1b). This membrane can help reduce the transmission of water vapor onto the sensor's surface, thus minimizing the influence of moisture on the sensor performance. The final device can be installed on the leaf surface with the help of a thin adhesive layer (Figure 1b). For monitoring methanol emission from a plant, the device is left on the leaf surface to accumulate gas emissions inside the chamber and provide an amperometric signal responding to the amount of the accumulated emission. Because all the sensor materials are flexible, the sensor has a conformable attachment to the leaf surface (Figure 1d). This work demonstrates that the sensor can detect methanol emission from the leaf of maize plants in both greenhouse and

https://doi.org/10.1021/acssensors.2c00834
ACS Sens. XXXX, XXX, XXX−XXX

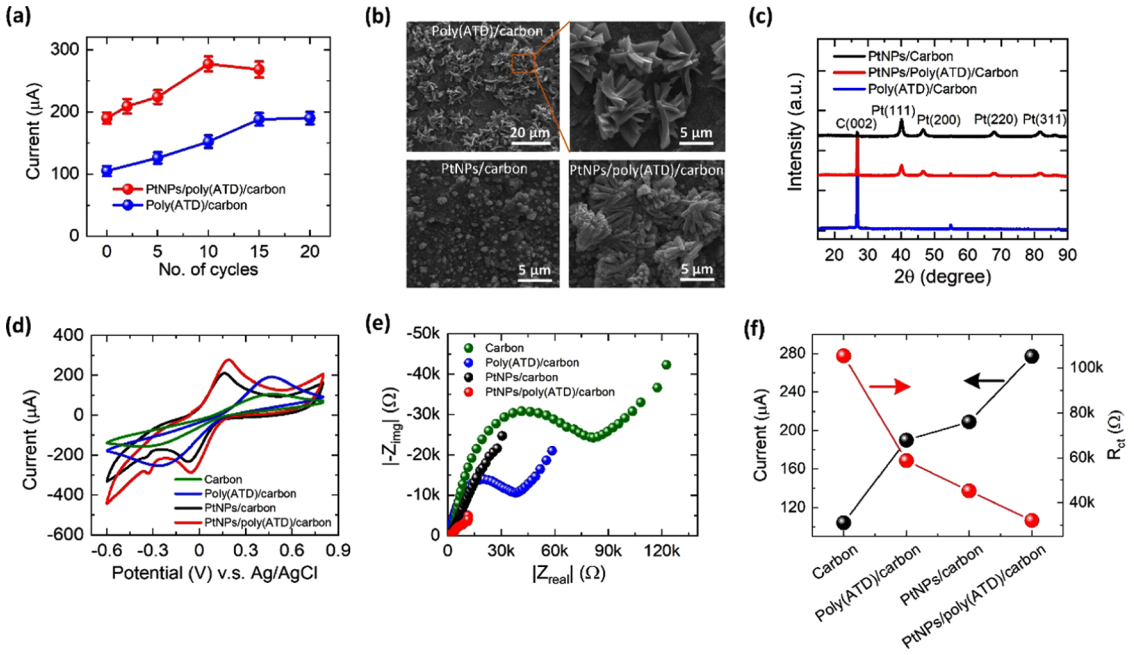

Figure 2. (a) Oxidation peak currents of the PtNPs/poly(ATD)/carbon and poly(ATD)/carbon electrodes as a function of the number of potentiodynamic cycles applied during the CV deposition in an electrolyte solution containing 1 mM $K_3[Fe(CN)_6]$ and 0.1 M KCl. (b) FESEM images of the poly(ATD)/carbon, PtNPs/carbon, and PtNPs/poly(ATD)/carbon electrodes. (c) X-ray diffraction (XRD) spectra of the poly(ATD)/carbon, PtNPs/carbon, PtNPs/poly(ATD)/carbon electrodes. (d, e) Cyclic voltammograms (d) and Nyquist plots (e) of the carbon, poly(ATD)/carbon, PtNPs/poly(ATD)/carbon, and PtNPs/carbon electrodes in the same redox electrolyte as that used in (a). The electrochemical impedance spectroscopy (EIS) measurement was conducted at the open circuit potential over the frequency range of 100 kHz to 10 MHz. (f) Oxidation peak current and charge transfer resistance R_{ct} for the four electrodes used in (d) and (e).

field and provide a noticeable difference in methanol emission between two genotypes of maize plants. Therefore, sensor technology will play a pivotal role in plant science by providing a new avenue to monitor an important molecular phenotype of plants.

2. EXPERIMENTAL SECTION

2.1. Materials. Poly(ethylene terephthalate) or PET (125 μm thickness) served as a flexible substrate of the sensor and was purchased from Sigma Aldrich (St. Louis, MO). To prepare a composite of PtNPs/poly(ATD), K_2PtCl_4 (98%) and ATD (97%) monomers were also purchased from Sigma Aldrich. To form a gas collection chamber, silicone epoxy was purchased from SmoothOn (Macungie, PA). Methanol, isopropanol alcohol, acetone, acetic acid, salicylic acid, and acetaldehyde were all purchased from Fisher Scientific (Hampton, NH) to characterize the sensor.

2.2. Preparation of PtNPs/Poly(ATD)/Carbon. Electropolymerization was used to deposit poly(ATD) on the surface of the carbon electrode by cyclic voltammetry (CV) on an electrochemical workstation (CH Instruments, Austin, TX). Figure S1a shows 20 cycles of CVs of the potentiodynamic polymerization of ATD in a mixture of 5 mM ATD and 0.1 M H_2SO_4 in a potential range from 0 to 1.2 V. Subsequently, PtNPs were electrodeposited on the obtained poly(ATD) by applying 15 potentiodynamic cycles in a potential window from −2.0 to +1.5 V in a solution containing 1 mM K_2PtCl_4 and 0.1 M H_2SO_4 (Figure S1b). In addition to PtNPs/poly(ATD)/carbon electrode, other counterpart electrodes, including carbon, poly(ATD)/carbon, and PtNPs/carbon electrodes, were also fabricated for control experiments.

2.3. Sensor Manufacturing. Three carbon-based electrodes (500 μm thickness; total ground carbon conductive coating; MG Chemicals, Burlington, ON, Canada) were formed on the surface of the PET substrate by a screen-printing method with the help of a stencil mask. The working electrode had a 10 mm diameter. A 500 μm-thick pseudo-reference electrode was realized by screen-printing Ag/AgCl paste on top of a carbon electrode. Another carbon electrode served as the counter electrode. The central carbon electrode was modified with the conducting poly(ATD) and PtNPs using the above-mentioned method. Next, a three-dimensional (3D)-printed mold was formed and filled with silicone liquid to fabricate the gas collection chamber. After thermally curing the silicone liquid on a hot plate at 55 °C for 4 h, the chamber was peeled out of the mold. Subsequently, the sensor was placed at the bottom of the chamber with an adhesive. Two hollow tubes (inner diameter: 150 μm; outer diameter: 250 μm; VitroCom, Mountain Lakes, NJ) were inserted through the chamber wall as the inlet and outlet of the collection chamber. These tubes were used to purge nitrogen (N_2) gas and vent residual gas. Finally, a hydrophobic gas diffusion membrane (poly(tetrafluoroethylene) or PTFE laminated membrane; 0.1 μm pore size; 47 mm diameter; Sterlitech, Auburn, WA) was used to cap the collection chamber, which allowed minimizing water vapor invasion into the chamber. Next, a Nafion perfluorinated resin solution (1 μm thickness; 5 wt % in a mixture of lower aliphatic alcohols and water; Sigma Aldrich, St. Louis, MO) was drop-casted on the sensor surface to serve as the electrolyte of the sensor. Therefore, the wearable VOC sensor was formed. The electrochemical characterization for the materials and sensors was performed on an electrochemical workstation (CH Instruments, Austin, TX).

3. RESULTS AND DISCUSSION

3.1. Material Characterization. The electropolymerization of ATD and the further deposition of PtNPs were optimized by adjusting the number of potentiodynamic cycles with the CV technique (Figure S1a,b; Supporting Information). The result shows that to obtain a high oxidation peak current, 15 cycles were required to deposit poly(ATD) on the surface of the carbon electrode and another 10 cycles to deposit PtNPs further (Figure 2a). Morphological studies were carried out using a field-emission scanning electron microscope (FESEM; FEI Quanta-FEG 250, Hillsboro, OR). The result

https://doi.org/10.1021/acssensors.2c00834
ACS Sens. XXXX, XXX, XXX−XXX

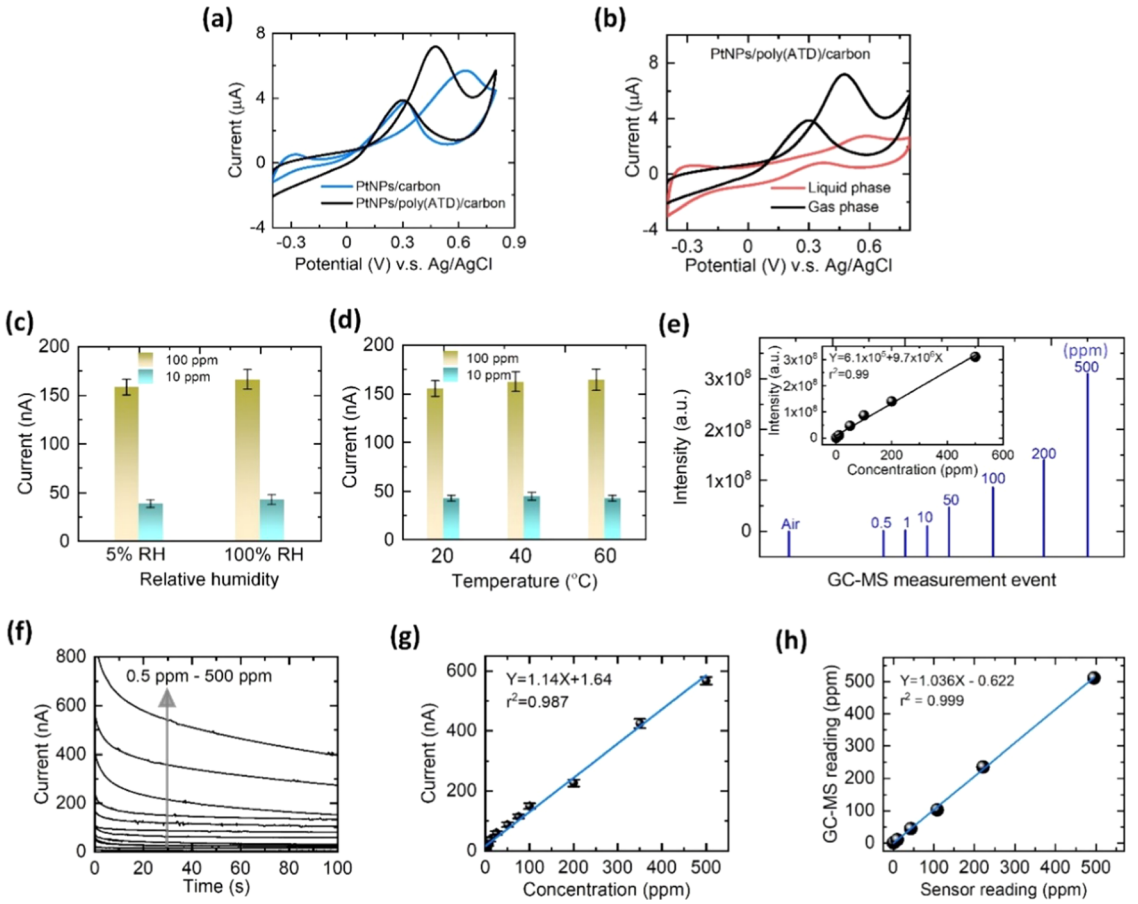

Figure 3. (a) Cyclic voltammograms of the PtNPs/poly(ATD)/carbon and PtNPs/carbon electrodes exposed to 1000 ppm concentration gas-phase methanol. (b) Cyclic voltammograms of the PtNPs/poly(ATD)/carbon electrode exposed to 1000 ppm methanol at liquid and gas phases. (c) Sensor response to 100 and 10 ppm concentration methanol at RH = 100 and 5%. (d) Sensor response to 100 and 10 ppm concentration methanol at 20, 40, and 60 °C. (e) GC-MS measurement for 0.5−500 ppm concentration methanol samples. The inset shows the peak intensity of GC-MS as a function of methanol concentration. (f) CA measurement of methanol using the sensor with PtNPs/poly(ATD)/carbon. (g) Peak current values from the CA curves in (f) as a function of methanol concentration. (h) GC-MS determined methanol concentration versus the sensor reading.

(Figure 2b) shows a flower-like microcrystallite structure of poly(ATD) on the surface of the base carbon electrode, as well as full coverage of PtNPs on the surface of poly(ATD).

The fabricated PtNPs/poly(ATD)/carbon, PtNPs/carbon, and poly(ATD)/carbon electrodes were examined by X-ray diffraction (XRD) spectroscopy (Siemens D500 X-ray diffractometer, Siemens, Karlsruhe, Germany) to confirm the presence of PtNPs on the surface of poly(ATD) (Figure 2c). The XRD patterns of the PtNPs/poly(ATD)/carbon and PtNPs/carbon had Bragg's reflection associated with crystalline platinum, as observed at 38.2, 44.4, 64.6, 77.5, and 81.8° which represented the (111), (200), (220), (311), and (222) planes, respectively, of FCC crystalline platinum (JCPDS PDF No. 70-0802). The diffraction peak at 26.2° was associated with carbon from the conducting polymer and the base carbon electrode. The crystalline size of PtNPs was calculated to be 10 ± 2 nm using the Scherrer formula based on the full width at half maximum at the primary peak.[33] The PtNPs were of finite size, and the aggregation of PtNPs is well controlled on the surface of poly(ATD).

Figure 2d shows the cyclic voltammograms of the PtNPs/poly(ATD)/carbon, PtNPs/carbon, poly(ATD)/carbon, and carbon electrodes using 1.0 mM $K_3[Fe(CN)_6]$ and 0.1 M KCl as the redox electrolyte. All the electrodes show typical Fe^{3+}/Fe^{2+} redox behaviors. Due to the distribution of the highly catalytic PtNPs on the surface of poly(ATD), the PtNPs/poly(ATD)/carbon electrode exhibited the highest peak current of 281 μA, compared with 213 μA for the PtNPs/carbon electrode, 195 μA for the poly(ATD)/carbon electrode, and 108 μA for the carbon electrode. The peak-to-peak potential differences ΔE for the PtNPs/poly(ATD)/carbon, PtNPs/carbon, poly(ATD)/carbon, and carbon electrodes are found to be 0.23, 0.24, 0.72, and 0.84 V, respectively. The lower ΔE values of the PtNPs/poly(ATD)/carbon and PtNPs/carbon electrodes infer the critical role of PtNPs in improving the catalytic activity of the sensing electrodes. Next, electrochemical impedance spectroscopy (EIS) was used to examine the interfacial electron transfer properties of these electrodes (Figure 2e). The Nyquist plots of the electrodes exhibited a semi-circular pattern followed by a linear plot and were fitted with the Randles equivalent circuit. The PtNPs/poly(ATD)/carbon electrode exhibited the highest electron-conducting behavior, as evident by the lowest charge transfer resistance R_{ct} of 31 kΩ, compared to 45 kΩ for the PtNPs/carbon electrode, 59 kΩ for the poly(ATD)/carbon electrode, and 106 kΩ for the carbon electrode. Figure 2f shows that the electrodes with lower R_{ct} values presented higher peak oxidation currents.

https://doi.org/10.1021/acssensors.2c00834
ACS Sens. XXXX, XXX, XXX−XXX

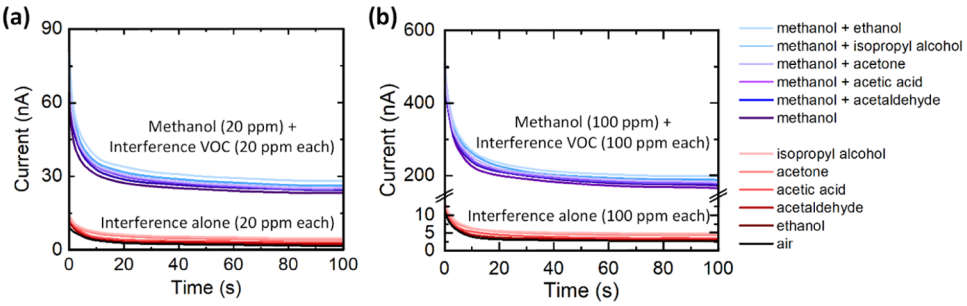

Figure 4. Selectivity test of the sensor with PtNPs/poly(ATD)/carbon in the presence of interference volatiles. The CA curves were obtained from the sensor in response to isopropyl alcohol, acetone, acetic acid, acetaldehyde, and ethanol with and without methanol, where each gas had a concentration of 20 ppm (a) and 100 ppm (b).

3.2. Sensor Characterization. The sensors with PtNPs/poly(ATD)/carbon and PtNPs/carbon were examined for electrochemical oxidation of gaseous methanol at 1000 ppm concentration using the CV technique (Figure 3a). The sensor with poly(ATD) exhibited a higher oxidation peak of 7.4 μA at a lower potential of 0.47 V than the counterpart with no conducting polymer (5.9 μA at 0.65 V). The enhanced electrocatalytic activity of PtNPs/poly(ATD)/carbon may be associated with strong linkages between PtNPs and the amine functional group of poly(ATD) that promoted facile electron transfer. Essentially, the extended p-orbital system of poly(ATD) could facilitate transferring the electrons from one end to the other end of this polymer, thus improving the electrocatalytic properties of the sensing electrode. Figure 3b shows that when the sensor with PtNPs/poly(ATD)/carbon was exposed to 1000 ppm liquid-phase methanol concentration, the oxidation of methanol occurred at a higher potential of 0.58 V than when the sensor was exposed to gaseous methanol of the same concentration.

Next, to examine the effect of relative humidity (RH) and temperature on the response of the sensor with PtNPs/poly(ATD)/carbon to gaseous methanol, the sensor was placed inside the gas collection chamber capped with the hydrophobic porous membrane (Figure 1b). Figure 3c shows that when the RH outside the collection chamber was set to be 100% RH and 5% RH, the sensor produced the oxidation current of 165 and 158 nA, respectively, in response to 100 ppm methanol concentration, while the sensor provided the current of 45 and 39 nA, respectively, in response to 10 ppm methanol concentration. Therefore, there existed only a negligibly small difference in the output current of the sensor under the two extreme RH conditions. This may possibly be due to the ability of the hydrophobic membrane to repel water vapor when gas molecules pass into the collection chamber of the sensor. The slight change in the oxidation current under the highly humid environment may be caused by the wettability of the Nafion-based electrolyte polymer of the sensor. Further, Figure 3d shows that as the environmental temperature varied from 20 to 60 °C, the output current of the sensor slightly increased by 3.3 and 5.4% when responding to 100 and 10 ppm concentration methanol, respectively. Therefore, the impact of RH and temperature on the sensor performance was relatively small, thus making it possible for on-site monitoring of methanol in the field.

Next, GC-MS analysis was conducted to validate the quantification of gaseous methanol using the PtNPs/poly(ATD)/carbon-based sensor over a wide concentration range of methanol from 0.5 to 500 ppm (Figure 3e). The intensity peak at 31.98 m/c in the GC-MS fingerprint signified methanol after removing the background signal associated with air (Figure S2). A calibration plot was constructed for the GC-MS data (the inset of Figure 3e), indicating a high correlation (r^2 = 0.99) between the peak intensity and methanol concentration. Further, a chronoamperometry (CA) study was carried out with the sensor, where the gaseous methanol of a known concentration was injected into an N_2-purged collection chamber of the sensor (Figure 3f). There appeared a linear relationship between the output current of the sensor (noted at 30 s for the CA measurement) and the methanol concentration under test, indicating a sensitivity of 1.14 nA/ppm with r^2 = 0.987 (Figure 3g). Further, for gaseous methanol samples with unknown concentrations, both the sensor and GC-MS methods were used to quantify these samples; the CA signals of the sensor measurement and the intensity peaks of the GC-MS measurement were converted to concentrations using the calibration plots in Figures 3g and 3e, respectively. A near-unity slope (slope = 1.036; r^2 = 0.999) was observed between the sensor output and GC-MS measurement (Figure 3i), indicating the high accuracy of the sensor in quantifying methanol.

Further, a selectivity test of the sensor with PtNPs/poly(ATD)/carbon was conducted with the CA technique in the presence of interfering volatiles, such as isopropyl alcohol, acetone, acetic acid, acetaldehyde, and ethanol. This experiment involved placing the sensor inside an electrochemical cell and flowing an individual interfering volatile compound or a mixture of methanol and interfering compound into the cell. Figure 4 shows the current responses of the sensor to the interfering volatiles with and without methanol, where each VOC had the same concentration (20 ppm in Figure 4a and 100 ppm in Figure 4b). The result indicates that the CA signals for the individual interferences alone were negligibly low (<5 nA). When exposed to a mixture of methanol and an individual interfering volatile with 20 ppm (or 100 ppm) concentration each, the sensor produced an output current of around 30 nA (or 200 nA), similar to that produced when the sensor was exposed to methanol with the same concentration alone. The result indicates that the CA signal due to methanol dominated over the interfering volatiles. Therefore, the sensor with PtNPs/poly(ATD)/carbon provided a considerable selectivity to methanol even in the presence of many interfering volatile compounds.

3.3. Plant Methanol Emission Measurement. First, the ability of the sensor to monitor methanol emission from the leaf of a maize plant in a greenhouse was tested. The sensor was installed at the back of a leaf using a thin adhesive layer.

https://doi.org/10.1021/acssensors.2c00834
ACS Sens. XXXX, XXX, XXX−XXX

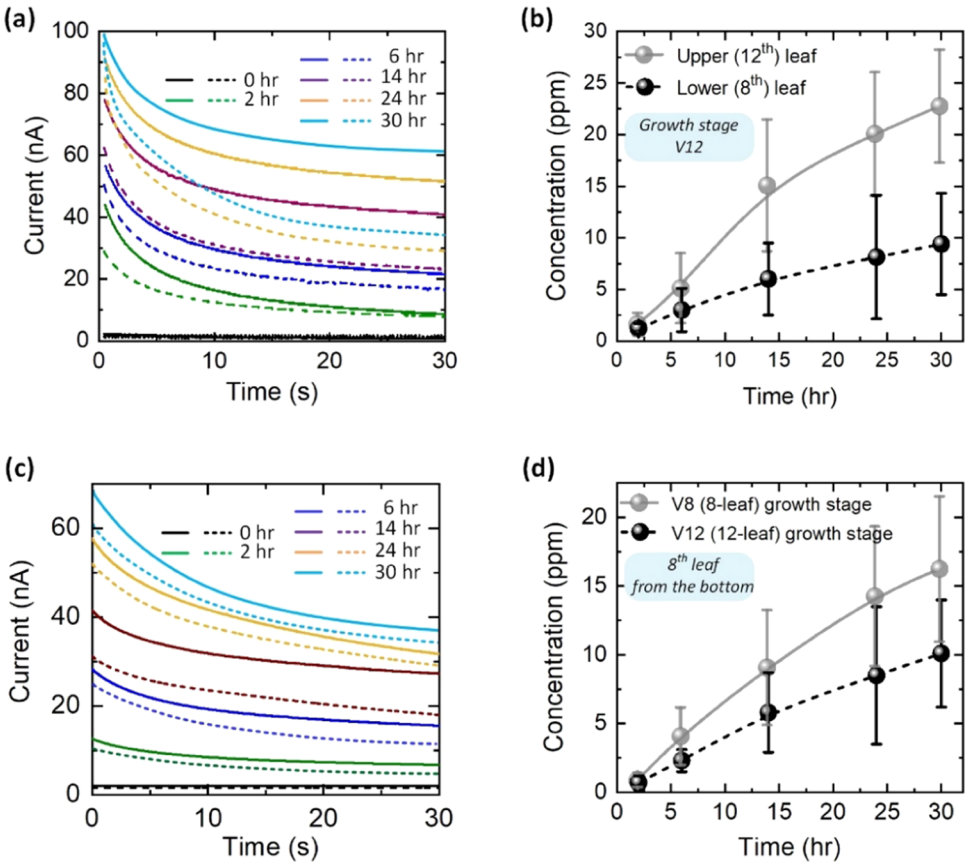

Figure 5. (a, b) CA curves (a) and methanol concentrations (b) obtained at different accumulation times using the sensors installed at the upper leaf (the 12th leaf from the bottom; solid lines) and the lower leaf (the 8th leaf; dashed lines) of a maize plant at the 12-leaf (V12) growth stage. (c, d) CA curves (c) and methanol concentrations (d) detected at different accumulation times using the sensor installed at the 8th leaf of the younger V8 growth stage plants (solid lines) and older V12 growth stage plants (dashed lines). Here, the collection chamber of the sensor was purged with N_2 gas at time $t = 0$.

The collection chamber of the sensor was purged with N_2 gas from a portable plastic bag through tubing with a controlled on/off switch. The inlet and outlet tubes were then sealed. As the sample accumulated, the sensor was used to measure methanol directly on the leaf surface at given accumulation times using the CA technique.

Sensors were used to identify a difference in methanol emission between a lower leaf and an upper leaf of a maize plant (the number of plants $n = 4$; genotype: B73; measured at the 12-leaf or V12 growth stage; Figure 5a,b) in the greenhouse. Specifically, the sensors were installed on the 8th (lower/older) leaf and the 12th (upper/younger) leaf from the bottom of the plant. The emitted samples were tested using the installed sensors at the accumulation times of 2, 6, 14, 24, and 30 h. Figure 5a shows that the output currents of the sensors at both the lower (dashed lines) and upper (solid lines) leaves increased with increasing accumulation time. Over 30 h (Figure 5b), the upper leaf had emitted a greater amount (concentration) of methanol (22.6 ± 5.7 ppm) than the lower leaf (9.4 ± 4.8 ppm); the rate of methanol accumulation slowed as the accumulation time increased, perhaps because the accumulated methanol inside the collection chamber negatively impacted the release of methanol from the leaf (i.e., negative feedback).

Next, sensors were attached to the 8th leaf (from the bottom) of maize plants at the V8 (8-leaf) and V12 (12-leaf) growth stages (the number of plants $n = 4$ of each stage; genotype: B73) in the greenhouse. The measurement result (Figure 5c,d) shows that older plants at the V12 growth stage emitted a smaller amount of methanol (10.2 ± 4.2 ppm at 30 h) than younger plants at the 8-leaf stage (16.4 ± 5.3 ppm at 30 h) (Figure 5d). Due to the higher metabolic activity, the young V8-stage plants could have greater methanol emissions than the mature V12-stage plants of the same genotype.

Further, a pilot experiment was conducted to validate the sensor in on-site monitoring of methanol emission from maize plants of two genotypes (Mo17 and B73 inbred lines) under field conditions at the Curtiss Farm of Iowa State University (Ames, Iowa) on July 25, 2021. The maize plants under test were at the 3-leaf (V3) growth stage. The sensor was attached to the back of the 3rd leaf and was then purged with N_2 gas from a portable bag. For each genotype, five random plants in a row were tested from each of 4 rows. Each measurement was conducted 2 h after purging. The result shows that at the V3 growth stage, the B73 genotype of maize emitted a greater concentration of methanol (51.4 ± 27.2 ppm) than the Mo17 genotype (34.5 ± 24.8 ppm) for 2 h of sample collection (Figure 6a). Much of the methanol produced by plants is a product of pectin methylesterases.[8] It is at least possible that the Mo17 and B73 genotypes differ in their accumulation or activities of these enzymes, resulting in different rates of methanol emission.

In addition, the sensor was used to conduct multiple measurements of methanol emission from the 3rd leaf of maize

https://doi.org/10.1021/acssensors.2c00834
ACS Sens. XXXX, XXX, XXX−XXX

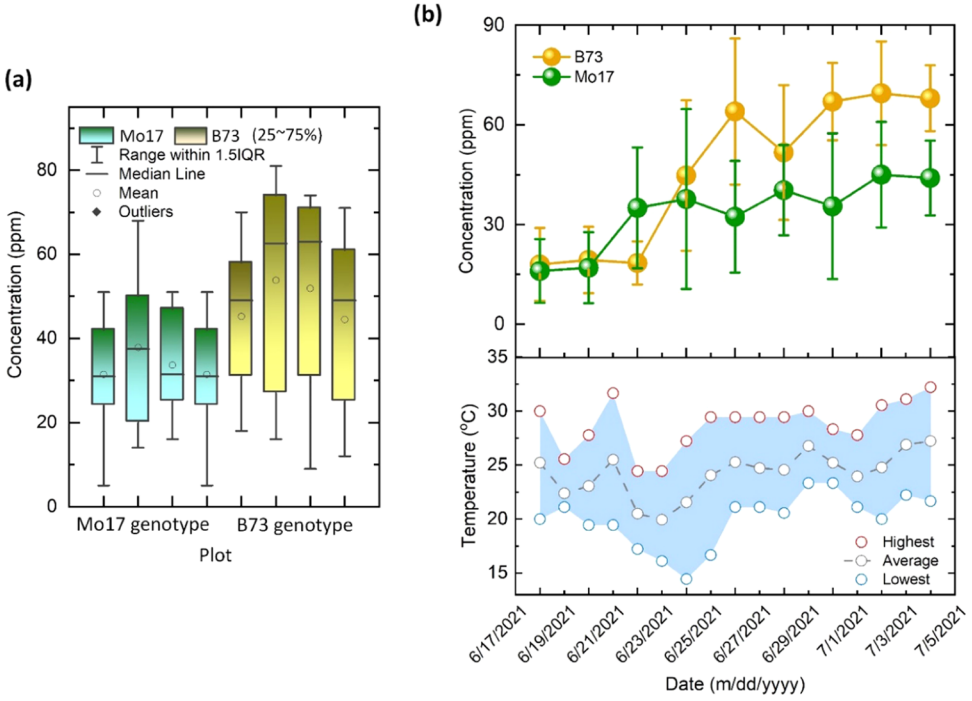

Figure 6. (a) Box plots for the concentration of methanol emission from maize plants of Mo17 and B73 genotypes. The measurement required a 2-h sample collection using the N_2-filled collection chamber of the sensor. (b) Changes in the concentration of methanol emission from maize plants of Mo17 and B73 genotypes at the Curtiss Farm of Iowa State University over 16 days from June 18, 2021 to July 4, 2021. The lower panel of (b) shows the daily temperature at the farm during the study period.

Table 1. Comparison of the Present Methanol Sensor with Other Methanol Sensors

sensor technology	sensing materials	detection limit (ppm)	response time (s)	dynamic range (ppm)	refs
fluorescence detection assisted with enzymatic conversion	methanol oxidase	0.01[a]	NA	NA	34
gas chromatography-mass spectrometry	NA	0.006[a]	NA	NA	35
chemoresistivity	indium tin oxide	0.1	NA	200−1800[b]	36
	Pd-doped SnO_2 nanoparticles assisted with separation column	0.0005	120	1−1000[a]	37
	tin oxide nanoflowers	1	4	200−400[a]	38
	stannous sulfide/reduced graphene oxide	0.25	NA	0.25−20[a]	39
	titanium dioxide/reduced graphene oxide	NA	18	10−80[a]	40
fiber-optics	sol silica and Nile red	0.281	300	0−200[a]	41
	bismuth tungstate	100	2100	0−500[a]	42
	carbon nanotubes	NA	6600	0−500[a]	43
amperometry	alcohol oxidase-peroxidase hybrid	0.32	120	0−6.4[a]	44
	quinoprotein methanol dehydrogenase enzyme	0.016	10	0.016−6.4[b]	45
quartz crystal microbalance	SiO_2 particles	0.001	300	0.001−100[a]	46
cyclic voltammetry	silicon epoxy coated Pt nanoparticles	3.2	200	9−319 800[b]	47
chronoamperometry	Pt/carbon nanotubes	1.6	22	6.4−319 800[b]	48
microwave waveguide	polyindole	0.06103	NA	5−500[a]	49
microwave split ring resonator	carbon nanotube coated fiber	100	32	100−300[a]	50
field-effect transistor	magnesium-doped indium tin oxide nanofiber	1	236	1−80[a]	51
chronoamperometry	PtNPs/poly(ATD)/carbon	0.5	10	0.5−500[a]	this work

[a]Gaseous methanol [b]Liquid-phase methanol

plants of Mo17 and B73 genotypes at the V3 growth stage in the field at the Curtiss Farm Iowa State University (Ames, Iowa) over 16 days from June 18, 2021 to July 4, 2021. The measurement frequency was set to be once every other day at the same time of the day, and each measurement was conducted after a 2-h sample collection in the N_2-filled collection chamber of the sensor (Figure 6b). After one measurement was completed, the chamber was purged with N_2 gas, and then the inlet and outlet of the chamber were left open until the next measurement cycle started. During the first 8 days (June 18 to June 26, 2021), the daily temperature fluctuated as large as 5 °C. The Mo17 genotype exhibited an increasing amount of methanol emission from 21.2 ± 9.3 to 32.6 ± 18.8 ppm. Similarly, for the B73 genomes, the amount

https://doi.org/10.1021/acssensors.2c00834
ACS Sens. XXXX, XXX, XXX−XXX

of methanol emission increased from 22 ± 9.5 to 63.7 ± 26.4 ppm. This increase in both genotypes likely reflects an increased metabolic activity over these 8 days that caused an increase in methanol emission from the plants. In the following days, from June 27 to July 24, 2021, the average daily temperature slightly fluctuated around 25°C. It was found that both Mo17 and B73 genotypes showed a reduced emission rate as the plants grew toward the V8-V9 growth stage, perhaps due to the slowing down of metabolic activity. Therefore, the sensor demonstrated its ability to distinguish methanol emission between different genotypes of maize plants.

Compared to other methanol detection methods (Table 1), the present sensor provided a wide dynamic range of methanol concentration (0.5−500 ppm) and a fast response time of 10 s with considerable selectivity and sensitivity to methanol due to the high catalytic activity and enhanced electron transfer ability of PtNPs/poly(ATD)/carbon. The wearable sensor design allowed direct monitoring of methanol emission from the leaf of a plant, representing a technological advancement in the sensors for plant physiology, as opposed to the traditional GC-MS approach that requires a complex sampling process, expensive instrument, and skilled operators. It should be noted that there remain some areas of improvement for the present sensor. For example, by incorporating wireless data transfer technology with the sensor, it is possible to enable an integrated wireless plant VOC sensor. Also, multiple sensing materials may be incorporated into the present wearable sensor platform to form an array of sensing elements for the simultaneous detection of multiple VOCs emitted from plants; this will help to better understand plant physiology under various conditions. Moreover, the sensing elements of the array will probe differential interactions of the elements with analytes. These interactions will generate measurable fingerprint patterns, which can be analyzed by pattern-recognition methods to classify the data to detect unknown samples. Machine learning algorithms have proven to be useful in analyzing such data. Recently, our group incorporated an artificial neural network to an array of three ion-selective sensing elements to improve the accuracy in detecting and quantifying, minimize the cross-sensitivity of these elements of the sensor, and thus improve the accuracy in measuring specific ions in the soils, plant tissues, and tile drainage water from crop fields.[52] A similar approach could be incorporated into a multimodal VOC sensor for characterizing the VOC emission fingerprints of plants. Such devices will help to understand volatile emission from plants, which is a key physiological parameter at the interface between plant responses and primary determinants of phenotype such as genotype.

4. CONCLUSIONS

We have developed a low-cost, field-deployable sensor to monitor methanol emissions from maize plants under field conditions. The sensor was featured using all flexible materials to achieve conformable attachment to the leaf surface. The ATD-based conducting polymer and PtNPs were sequentially deposited on the surface of a carbon electrode through the electrodeposition method to form a highly sensitive and selective sensing material for the detection and quantification of gaseous methanol. Both the laboratory and in-field measurements were conducted with the sensor, demonstrating an excellent ability of the sensor to monitor methanol emission from the leaf of a maize plant. The present wearable sensor will be useful for a better understanding of the physiological status, stress, and health of crops in field conditions. As a new portable sensor for plant methanol emission, this sensor technology is promising to solve the problems facing the existing volatile measurement approaches, thus making a more significant impact in plant sciences and agronomy.

■ ASSOCIATED CONTENT

Supporting Information

The Supporting Information is available free of charge at https://pubs.acs.org/doi/10.1021/acssensors.2c00834.

Details of electrochemical deposition for poly(ATD) and PtNPs on the surface of the working electrode. Gas chromatography-mass spectroscopy (GC-MS) measurement results for verifying the accuracy of the sensor in measuring methanol samples (PDF)

■ AUTHOR INFORMATION

Corresponding Author

Liang Dong − *Department of Electrical and Computer Engineering, Iowa State University, Ames, Iowa 50011, United States;* orcid.org/0000-0002-0967-4955; Phone: +1(515)294-0388; Email: ldong@iastate.edu

Authors

Hussam Ibrahim − *Department of Electrical and Computer Engineering, Iowa State University, Ames, Iowa 50011, United States;* orcid.org/0000-0003-0458-3795

Satyanarayana Moru − *Department of Electrical and Computer Engineering, Iowa State University, Ames, Iowa 50011, United States;* orcid.org/0000-0003-4301-0383

Patrick Schnable − *Agronomy Department, Iowa State University, Ames, Iowa 50011, United States*

Complete contact information is available at: https://pubs.acs.org/10.1021/acssensors.2c00834

Author Contributions

[§]H.I. and S.M. contributed equally. L.D. conceived the sensor concept and designed the experiments. H.I. and S.M. performed the experiments and prepared the figures. P.S.S. analyzed the data obtained from measurements with plants. L.D. supervised research. All authors wrote the manuscript.

Notes

The authors declare no competing financial interest.

■ ACKNOWLEDGMENTS

This work was supported in part by the U.S. Department of Agriculture (USDA) under grant numbers 2018-67021-27845, 2020-67021-31528, and 2020-68013-30934; in part by the U.S. National Science Foundation (NSF) under grant numbers CNS-2125484 and IOS-1844563; in part by the AI Research Institutes program supported by NSF and USDA-NIFA under AI Institute for Resilient Agriculture under grant number 2021-67021-35329. The seed funding for this research was from the Plant Sciences Institute at Iowa State University. The authors claim that there is no conflict of interest and share equal contributions. The authors thank Lisa Coffey of the Schnable Lab for her assistance with plant care.

■ REFERENCES

(1) Chu, M.; Nguyen, T.; Pandey, V.; Zhou, Y.; Pham, H. N.; Bar-Yoseph, R.; Radom-Aizik, S.; Jain, R.; Dan, M. C.; Khine, M.

Respiration rate and volume measurements using wearable strain sensors. *NPJ Digital Medicine* **2019**, *2*, No. 8.
(2) Sheikh, I.; Mahgoub, I.; Du, E.; Leavitt, M. A.; Asghar, W. Advances in healthcare wearable devices. *npj Flexible Electron.* **2021**, *5*, 1−14.
(3) Qaim, M. Role of new plant breeding technologies for food security and sustainable agricultural development. *Appl. Econ. Perspect. Policy* **2020**, *42*, 129−150.
(4) Oren, S.; Ceylan, H.; Schnable, P. S.; Dong, L. High-resolution patterning and transferring of graphene-based nanomaterials onto tape toward roll-to-roll production of tape-based wearable sensors. *Adv. Mater. Technol.* **2017**, *2*, No. 1700223.
(5) Yoon, I.; Eom, G.; Lee, S.; Kim, B. K.; Kim, S. K.; Lee, H. J. A capacitive micromachined ultrasonic transducer-based resonant sensor array for portable volatile organic compound detection with wireless systems. *Sensors* **2019**, *19*, 1401.
(6) Liu, S. F.; Lionel CH, M.; Timothy, M. S. Single-walled carbon nanotube−metalloporphyrin chemiresistive gas sensor arrays for volatile organic compounds. *Chem. Mater.* **2015**, *27*, 3560−3563.
(7) Wong, M. H.; Hao, J. P.; Giraldo, S.-Y.; Kwak, V. B.; Koman, R.; Sinclair, T.; Thomas Salim Lew, G.; Bisker, P. L.; Strano, M. S. Nitroaromatic detection and infrared communication from wild-type plants using plant nanobionics. *Nat. Mater.* **2017**, *16*, 264−272.
(8) Dorokhov, Y. L.; Ekaterina, V. S.; Tatiana, V. K. Methanol in plant life. *Front. Plant Sci.* **2018**, *9*, No. 1623.
(9) Vivaldo, G.; Masi, E.; Taiti, C.; Caldarelli, G.; Mancuso, S. The network of plants volatile organic compounds. *Scientific Reports* **2017**, *7*, No. 11050.
(10) Randon, J.; Maret, L.; Corinne, F. Gas chromatography−mass spectroscopy optimization by computer simulation, application to the analysis of 93 volatile organic compounds in workplace ambient air. *Anal. Chim. Acta* **2014**, *812*, 258−264.
(11) Blake, R. S.; Paul, M.; Andrew, M. E. Proton-transfer reaction mass spectrometry. *Chem. Rev.* **2009**, *109*, 861−896.
(12) Tabassum, S.; Kumar, R.; Dong, L. Plasmonic crystal-based gas sensor toward an optical nose design. *IEEE Sens. J.* **2017**, *17*, 6210−6223.
(13) Alinoori, A. H.; Masoum, S. Multicapillary gas chromatography—Temperature modulated metal oxide semiconductor sensors array detector for monitoring of volatile organic compounds in closed atmosphere using gaussian apodization factor analysis. *Anal. Chem.* **2018**, *90*, 6635−6642.
(14) Conti, P. P.; Rafaela, S. A.; Mercante, L. A.; Fugikawa-Santos, L.; Correa, D. S. Discriminative detection of volatile organic compounds using an electronic nose based on TiO2 hybrid nanostructures. *Sens. Actuators, B* **2021**, *344*, No. 130124.
(15) Shi, W.; Huo, X.; Tian, Y.; Lu, X.; Yang, L.; Zhou, Q.; Wang, X.; Yu, Q. Development of membrane inlet photoionization ion trap mass spectrometer for trace VOCs analysis. *Talanta* **2021**, *230*, No. 122352.
(16) Wei-Hao Li, M.; Ghosh, A.; Venkatasubramanian, A.; Sharma, R.; Huang, X.; Fan, X. High-sensitivity micro-gas chromatograph−photoionization detector for trace vapor detection. *ACS Sens.* **2021**, *6*, 2348−2355.
(17) Romih, T.; Menart, E.; Jovanovski, V.; Jerič, A.; Andrensek, S.; Hočevar, S. B. Sodium-polyacrylate-based electrochemical sensors for highly sensitive detection of gaseous phenol at room temperature. *ACS Sens.* **2020**, *5*, 2570−2577.
(18) Tung, T. T.; Thanh, M. T.; Tran, J.-F.; Feller, M.; Castro, T. V.; Ngo, K.; Hassan, M. J. N.; Losic, D. Graphene and metal organic frameworks (MOFs) hybridization for tunable chemoresistive sensors for detection of volatile organic compounds (VOCs) biomarkers. *Carbon* **2020**, *159*, 333−344.
(19) Li, Z.; Paul, R.; Ba Tis, T.; Saville, A. C.; Hansel, J. C.; Yu, T.; Ristaino, J. B.; Wei, Q. Non-invasive plant disease diagnostics enabled by smartphone-based fingerprinting of leaf volatiles. *Nat. Plants* **2019**, *5*, 856−866.
(20) Yin, S.; Ibrahim, H.; Schnable, P. S.; Castellano, M. J.; Dong, L. A field-deployable, wearable leaf sensor for continuous monitoring of vapor-pressure deficit. *Adv. Mater. Technol.* **2021**, *6*, No. 2001246.
(21) Giraldo, J. P.; Wu, H.; Newkirk, G. M.; Kruss, S. Nanobiotechnology approaches for engineering smart plant sensors. *Nat. Nanotechnol.* **2019**, *14*, 541−553.
(22) Moru, S.; Ibrahim, H.; Dong, L. In *Wearable Sensors for On-Leaf Monitoring of Volatile Organic Compounds Emissions from Plants*, 2020 IEEE 15th International Conference on Nano/Micro Engineered and Molecular System (NEMS); IEEE, 2020; pp 565−570.
(23) Li, Z.; Liu, Y.; Hossain, O.; Paul, R.; Yao, S.; Wu, S.; Ristaino, J. B.; Zhu, Y.; Wei, Q. Real-time monitoring of plant stresses via chemiresistive profiling of leaf volatiles by a wearable sensor. *Matter* **2021**, *4*, 2553−2570.
(24) Harley, P.; Greenberg, J.; Niinemets, Ü.; Guenther, A. Environmental controls over methanol emission from leaves. *Biogeosciences* **2007**, *4*, 1083−1099.
(25) Wu, S. C.; Zhang, Yi. Active DNA demethylation: many roads lead to Rome. *Nat. Rev. Mol. Cell Biol.* **2010**, *11*, 607−620.
(26) Dorokhov, Y. L.; Tatiana, V. K.; Petrunia, I.r V.; Frolova, O. Y.; Pozdyshev, D. V.; Gleba, Y. Y. Airborne signals from a wounded leaf facilitate viral spreading and induce antibacterial resistance in neighboring plants. *PLoS Pathog.* **2012**, *8*, No. e1002640.
(27) Nemecek-Marshall, M.; Robert, C. M.; Franzen, J. J.; Wojciechowski, C. L.; Fall, R. Methanol emission from leaves (enzymatic detection of gas-phase methanol and relation of methanol fluxes to stomatal conductance and leaf development). *Plant Physiol.* **1995**, *108*, 1359−1368.
(28) Yamagiwa, H.; Sato, S.; Fukawa, T.; Ikehara, T.; Maeda, R.; Mihara, T.; Kimura, M. Detection of volatile organic compounds by weight-detectable sensors coated with metal-organic frameworks. *Sci. Rep.* **2014**, *4*, No. 6247.
(29) Hu, Y.; Li, C.-Y.; Wang, X.-M.; Yang, Y.-H.; Zhu, H.-L. 1, 3, 4-Thiadiazole: synthesis, reactions, and applications in medicinal, agricultural, and materials chemistry. *Chem. Rev.* **2014**, *114*, 5572−5610.
(30) Tripković, A.; Dj Popović, K.; Grgur, B. N.; Blizanac, B.; Ross, P. N.; Marković, N. M. Methanol electrooxidation on supported Pt and PtRu catalysts in acid and alkaline solutions. *Electrochim. Acta* **2002**, *47*, 3707−3714.
(31) Iwasita, T. Electrocatalysis of methanol oxidation. *Electrochim. Acta* **2002**, *47*, 3663−3674.
(32) Zhai, D.; Liu, B.; Shi, Y.; Pan, L.; Wang, Y.; Li, W.; Zhang, R.; Yu, G. Highly sensitive glucose sensor based on Pt nanoparticle/polyaniline hydrogel heterostructures. *ACS Nano,* **2013**, *7*, 3540−3546.
(33) Patterson, A. L. The Scherrer formula for X-ray particle size determination. *Phys. Rev.* **1939**, *56*, 978.
(34) Nemecek-Marshall, M.; Robert, C. M.; Franzen, J. J.; Wojciechowski, C. L.; Fall, R. ″Methanol emission from leaves (enzymatic detection of gas-phase methanol and relation of methanol fluxes to stomatal conductance and leaf development). *Plant Physiol.* **1995**, *108*, 1359−1368.
(35) MacDonald, R. C.; Fall, R. Detection of substantial emissions of methanol from plants to the atmosphere. *Atmos. Environ., Part A* **1993**, *27*, 1709−1713.
(36) Patel, N. G.; Patel, P. D.; Vaishnav, V. S. Indium tin oxide (ITO) thin film gas sensor for detection of methanol at room temperature. *Sens. Actuators, B* **2003**, *96*, 180−189.
(37) Broek, J.; Abegg, S.; Pratsinis, S. E.; Güntner, A. T. Highly selective detection of methanol over ethanol by a handheld gas sensor. *Nat. Commun.* **2019**, *10*, No. 4220.
(38) Song, L.; Lukianov, A.; Butenko, D.; Li, H.; Zhang, J.; Feng, M.; Liu, L.; Chen, D.; Klyui, N. I. Facile synthesis of hierarchical tin oxide nanoflowers with ultra-high methanol gas sensing at low working temperature. *Nanoscale Res. Lett.* **2019**, *14*, No. 84.
(39) Qin, Y.; Wang, J.; Bai, Y. Graphene-Oriented Construction of 2D SnS for Methanol Gas-Sensor Application. *Phys. Status Solidi A* **2021**, *218*, No. 2000642.

https://doi.org/10.1021/acssensors.2c00834
ACS Sens. XXXX, XXX, XXX−XXX

(40) Acharyya, D.; Bhattacharyya, P. Highly efficient room-temperature gas sensor based on TiO 2 nanotube-reduced graphene-oxide hybrid device. *IEEE Electron Device Lett.* **2016**, *37*, 656−659.
(41) Liu, D.; Kumar, R.; Wei, F.; Han, W.; Mallik, A. K.; Yuan, J.; Wan, S.; He, X.; Kang, Z.; Li, F.; Yu, C.; Farrell, G.; Semenova, Y.; Wu, Q. High sensitivity optical fiber sensors for simultaneous measurement of methanol and ethanol. *Sens. Actuators, B* **2018**, *271*, 1−8.
(42) Maricar, S. M.; ManjoorShaib, D.; Sastikumar, P.; Reddy, V.; Ashok, M. Fiber optic gas sensor response of hydrothermally synthesized nanocrystalline bismuth tungstate to methanol. *Mater. Lett.* **2021**, *288*, No. 129337.
(43) Manivannan, S.; Saranya, A. M.; Renganathan, B.; Sastikumar, D.; Gobi, G.; Chang Park, Kyu. Single-walled carbon nanotubes wrapped poly-methyl methacrylate fiber optic sensor for ammonia, ethanol and methanol vapors at room temperature. *Sens. Actuators, B* **2012**, *171−172*, 634−638.
(44) Hasunuma, T.; Kuwabata, S.; Fukusaki, E.-i.; Kobayashi, A. Real-time quantification of methanol in plants using a hybrid alcohol oxidase− peroxidase biosensor. *Anal. Chem.* **2004**, *76*, 1500−1506.
(45) Liu, Q.; Kirchhoff, J. R. Amperometric detection of methanol with a methanol dehydrogenase modified electrode sensor. *J. Electroanal. Chem.* **2007**, *601*, 125−131.
(46) Xie, J.; Zhang, L.; Xing, H.; Bai, P.; Liu, B.; Wang, C.; Lei, K.; Wang, H.; Peng, S.; Yang, S. Gas sensing of ordered and disordered structure SiO2 and their adsorption behavior based on quartz crystal microbalance. *Sens. Actuators, B* **2020**, *305*, No. 127479.
(47) Park, D.-S.; Won, M.-S.; Goyal, R. N.; Shim, Y.-B. The electrochemical sensor for methanol detection using silicon epoxy coated platinum nanoparticles. *Sens. Actuators, B* **2012**, *174*, 45−50.
(48) Xu, J.; Wang, S.; Du, Z.; Zhu, J.; Liu, Y.; Zhang, W.; Wang, J. Electrochemical detection of methanol by platinum/carbon nanotubes nanocomposites synthesised via hydrogen plasma reduction process. *Micro Nano Lett.* **2013**, *8*, 890−894.
(49) Kumar, A.; Wang, C.; Meng, F.-Y.; Jiang, C.-P.; Yan, G.-F.; Zhao, M.; Jing, C.-Q.; Wang, L. Ultrafast detection and discrimination of methanol gas using a polyindole-embedded substrate integrated waveguide microwave sensor. *ACS Sens.* **2020**, *5*, 3939−3948.
(50) Singh, S. K.; Azad, P.; Akhtar, M. J.; Kar, K. K. Improved methanol detection using carbon nanotube-coated carbon fibers integrated with a split-ring resonator-based microwave sensor. *ACS Appl. Nano Mater.* **2018**, *1*, 4746−4755.
(51) Li, L.; Li, J.; Fu, W.; Jiang, D.; Song, Y.; Yang, Q.; Zhu, W.; Zhang, J. Mg-doped InSnO nanofiber field-effect transistor for methanol gas detection at room temperature. *Nanotechnology* **2022**, *33*, No. 205502.
(52) Chen, Y.; Tang, Z.; Zhu, Y.; Castellano, M. J.; Dong, L. Miniature multi-ion sensor integrated with artificial neural network. *IEEE Sens. J.* **2021**, *21*, 25606−25615.

https://doi.org/10.1021/acssensors.2c00834
ACS Sens. XXXX, XXX, XXX−XXX